Material Incorporation Inside Single-Walled Carbon Nanotubes Using Plasma-Ion Irradiation Method

Rikizo Hatakeyama, Goo-Hwan Jeong, and Takamichi Hirata

***Abstract*—An original approach using plasma technology has been performed in order to develop novel functional nanocarbons such as fullerenes (C_{60}) and carbon nanotubes. Fully ionized plasmas, which consist of alkali positive ions, fullerene negative ions, and a small fraction of residual electrons have been produced. When positive or negative bias voltages are applied to single-walled carbon nanotubes (SWNTs) in the plasmas, accelerated negative fullerene or positive alkali-metal ions are irradiated to the SWNTs, respectively. In contrast to pristine samples, a remarkable structural change of the nanotubes is observed after the plasma-ion irradiation. Especially, Cs encapsulation inside the SWNTs is directly observed by field-emission transmission electron microscopy (TEM) and scanning TEM. On the other hand, the fullerene encapsulated SWNTs are successfully formed by fullerene-ion irradiation. In addition to this material incorporation, structural modification such as tube opening is also observed and supposed to occur by momentum transfer from ions to nanotubes. Finally, our method using plasma technology is expected to provide a nanotechnology alternative to conventional chemical process, creating a new possibility for the novel functional nanomaterial synthesis.**

***Index Terms*—Cesium, encapsulation, fullerenes, ion radiation effects, nanotechnology, plasma measurements, single-walled carbon nanotubes (SWNTs).**

I. Introduction

AFTER THE discovery of the buckminsterfullerene C_{60} in 1985 [1], which led to a Nobel Prize in chemistry in 1996, by a collaboration of Smalley *et al.*, extensive relevant works have been carried out due to the brand-new chemistry and condensed physics originated from zero-dimensional structure. In addition, multiwalled (MW) [2] and single-walled carbon nanotubes (SWNTs) [3], which are formed by rolled graphene sheets and were discovered by Iijima in 1993 and 1991, respectively, also become a subject of intensive investigation due to their one-dimensional structural uniqueness and potential applications to many fields. It is especially very attractive that intrinsic electronic and mechanical properties of carbon nanotubes can be controlled by introduction of various foreign atoms, molecules, and their derivatives [4]–[6]. For example, the recent report has presented the possibility of a nanoscale electronic device for the case of intercalation of a (alkali metal/halogen element) junction inside the SWNTs [7].

On the other hand, much interest in various fields of physics and engineering has also been concentrated on plasmas including dusts or fine particles. Among others, ultrafine particle plasmas might also be very attractive from the standpoint of material science because they could inspire numerous possibilities of developing novel-structured nanomaterials.

Here, in order to realize the one-dimensional novel structure mentioned above, we attempt to perform an interdisciplinary original approach of ion irradiation using different-polarity ion plasmas, where various types of atoms, molecules, or their combinations could be selectively encapsulated within carbon nanotubes. As a result, we present the validity of our plasma method and focus on the successful formation of the SWNTs encapsulating alkali metals, as well as fullerene molecules.

Manuscript received August 8, 2003; revised December 29, 2003. This work was supported in part by the Ministry of Education, Culture, Sports, Science, and Technology, Japan under a Grant-in-Aid for Scientific Research and by the Research Institute of Electrical Communication, Tohoku University under the Cooperative Research Project Program. This paper was presented in part at IEEE-NANO2003, San Francisco, CA, August 12–14, 2003.

The authors are with the Department of Electronic Engineering, Tohoku University, Sendai 980-8579, Japan (e-mail: hatak17@ec.ecei.tohoku.ac.jp).

Digital Object Identifier 10.1109/TNANO.2004.828517

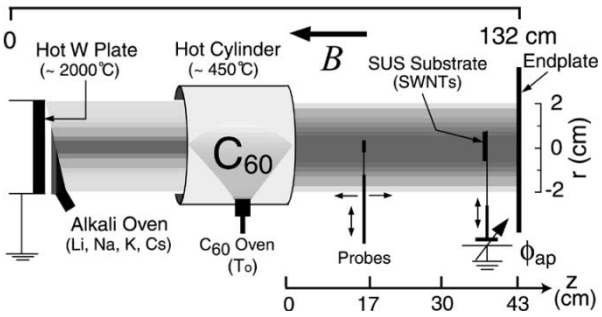

Fig. 1. Schematic illustration of experimental setup.

II. Experimental Details

A. Alkali–Fullerene Plasma Production

The production of different-polarity ion plasma and their irradiation experiment are carried out using a single-ended Q machine [8] with a vacuum chamber of 10-cm diameter and 132-cm length, as shown in Fig. 1. The low-temperature alkali-metal plasma is produced by surface contact ionization of alkali metals (Li, Na, K, or Cs) on a hot 2.0-cm-diameter tungsten plate, which emits electrons according to the Richardson–Dushman law under the background pressure of $(1\text{–}3) \times 10^{-6}$ torr and flows along magnetic-field lines ($\mathbf{B} = 0.2$ T) toward an endplate situated at a distance of 43 cm from the hot-cylinder edge. The density and electron temperature of this alkali-metal plasma ($Li^+ - e^-$, $Na^+ - e^-$, $K^+ - e^-$ or $Cs^+ - e^-$) are measured to be $n_e = 1 \times 10^8$–10^{10} cm^{-3} and $T_e \approx 0.2$ eV ($\geq$ positive-ion temperature) by a Langmuir probe, respectively.

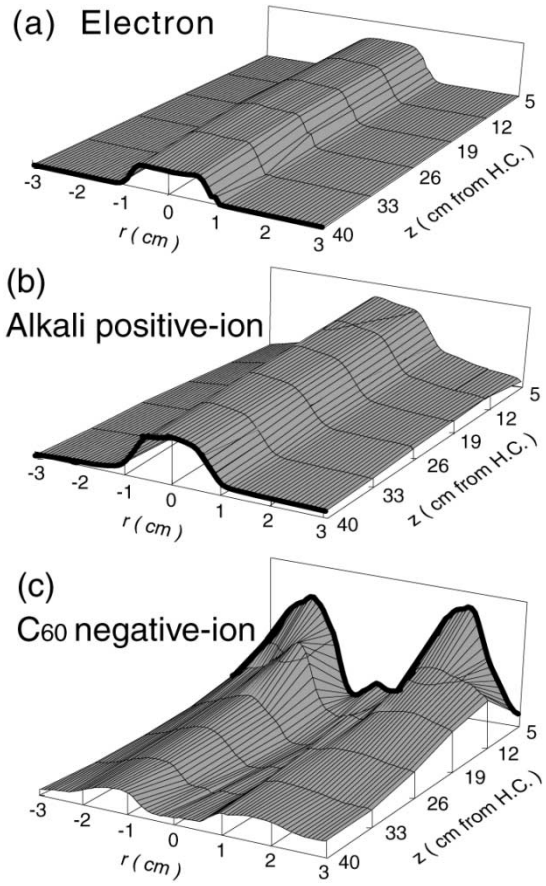

Fig. 2. Two-dimensional (r–z) density profiles of: (a) electrons, (b) alkali positive ions, and (c) C_{60} negative ions for $T_o = 500$ °C.

In order to produce C_{60} negative ions, a coaxial copper cylinder (6-cm diameter and 20-cm length) with a heating system and a side hole (3-mm diameter), through which the fullerene particles are injected, is installed in the middle of the alkali-metal plasma column. The monitoring of sublimated fullerene particles is carried out by measuring a negative saturation current, which depends on the temperature T_o of C_{60} sublimation oven of the Langmuir probe at the radial center. The fullerene powder filled in the sublimation oven, which is installed inside the side hole of the hot (∼450 °C) copper cylinder, has a high purity of 99.5+% (MTR Ltd.). When the oven temperature is raised up to 500 °C, electron attachment to sublimated C_{60} molecules $(C_{60} + e^- \rightarrow C_{60}^-)$ takes place in the alkali-metal plasma due to relatively high electron affinity of C_{60} (≈2.65 eV). The electron fraction $1 - \varepsilon(=n_e/n_+)$ is calculated by a value of n_e/n_{e0}, where n_e, n_+, and n_{e0} are electron and positive ion densities of an alkali–fullerene plasma, and electron density of the alkali plasma before the fullerene introduction, respectively.

As a result of electron attachment increasing with an increase in T_o (=200 °C → 500 °C), the radial density profile of the plasma in a downstream region from the hot-cylinder edge ($z > 0$) is strongly modified, as presented in Fig. 2, where two-dimensional (r–z) measurements are performed in the case of $T_o = 500$ °C. Fig. 2(a) shows the profiles of the negative-saturation current of the Langmuir probe, where a decrease of the electron density fraction is observed and electrons are found to

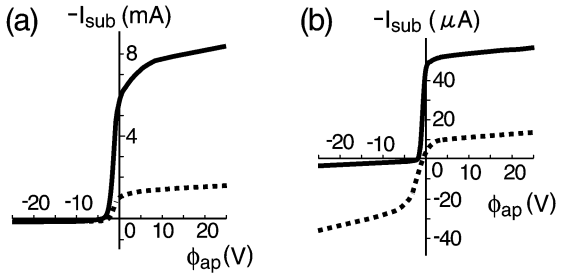

Fig. 3. Typical substrate current–voltage characteristics obtained in the: (a) plasma core region ($|r| = 0$ cm) and (b) its periphery region ($|r| = 1.5$ cm). The black lines correspond to the case of alkali-metal plasma and the dotted lines correspond to the case of alkali–fullerene plasma.

be well confined within the hot-plate diameter ($|r| < 1$ cm). On the other hand, the radial profiles of the positive-saturation current of the probe indicate that positive ions radially diffuse further beyond ($|r| > 1$ cm) the core plasma region [see Fig. 2(b)]. In order to measure the radial profiles of fullerene negative ions, bias voltages applied to electrodes of an ion sensitive probe [9] are carefully adjusted so as to prevent electrons from flowing into a collector of the probe. The C_{60} negative ions tend to be preferentially distributed beyond the core region and pronounced peaks in the radial profile appear in the periphery region ($|r| > 1$ cm), as shown in Fig. 2(c). This diffusion nature of C_{60} negative ions results in the spatial density decrease along the magnetic-field lines. In the end, the alkali–fullerene plasma ($Li^+ - C_{60}^-$, $Na^+ - C_{60}^-$, $K^+ - C_{60}^-$, or $Cs^+ - C_{60}^-$) with a very small fraction of the electron density is generated downstream from the hot cylinder region.

B. Plasma Characteristics

Fig. 3 presents typical current $(I_{\rm sub})$-voltage characteristics of a substrate inserted into the plasma, to which dc-bias voltages $(\phi_{\rm ap})$ are applied with respect to the grounded hot plate. In comparison with the case of the alkali-metal plasma (black lines), the negative-saturation current of the characteristic apparently decreases around the plasma core region (Fig. 2(a), $|r| = 0$ cm), but the positive-saturation current highly increases in the periphery region (Fig. 2(b), $|r| = 1.5$ cm) in the case of the alkali–fullerene plasma (dotted lines). This result indicates that the alkali–fullerene plasma is radially diffused in the axial magnetic field due to large Larmor radii r_L ($=mv_\perp/eB$; m: ion mass, $v_\perp$: ion velocity perpendicular to B, e: electron charge), of C_{60} negative ions ($r_L = 4.65$ mm) with the mass much larger than that of alkali-metal positive ions ($r_L = 0.85, 1.54, 2.01$, and 3.71 mm for Li, Na, K, and Cs, respectively), being almost electron free in the periphery region. Thus, positively and negatively charged particles are substantially accelerated by sheaths [10] in front of the substrate for $\phi_{\rm ap} < 0$ and $\phi_{\rm ap} > 0$, respectively, flowing into the SWNT bundles.

C. Nanotube Preparation and Plasma-Ion Irradiation

SWNTs prepared by an arc discharge method were mainly used in this study. As the comparison materials, double-walled carbon nanotubes (DWNTs) [11] and multiwalled carbon nanotubes (MWNTs) [12] were also used in order to clearly demonstrate the plasma-ion irradiation effects. Actually, a little

portion of triple-walled nanotubes (TWNTs) or MWNTs is still contained in the DWNT's powder which are produced by arc discharge and purified. The SWNTs purified by HIDE method [13] were dispersed by brief sonication in ethanol. Then, droplets of this suspension were dripped and dried on the stainless steel substrates (1.5 cm × 1.5 cm). The substrate is immersed in the plasma column as already shown in Fig. 1. All plasma-ion irradiation experiments are performed for 1 hour. Field-emission scanning electron microscopy (FE SEM) (Hitachi S-4100) and field-emission gun transmission electron microscopy (FE TEM) (Hitachi HF-2000) operating at 200 kV and having a point-to-point resolution of 0.23 nm are used for the structural characterization of nanotubes. Energy dispersive X-ray spectrometry (EDS) (Noran Instruments) is also utilized for the chemical element detection. Purified and ion irradiated SWNTs are also characterized by Raman scattering spectroscopy (Jovin Yvon T-64000) using an Ar ion laser at a wavelength of 488 nm. In case of the Cs irradiation, the Z-contrast technique by scanning transmission electron microscopy (STEM) (Hitachi HD-2000), which is capable of chemical elements mapping under the nanometer scale, is adopted for the purpose of confirming the existence of Cs inside carbon nanotubes.

III. Results and Discussion

A. Alkali-Metal Plasma-Ion Irradiation to SWNTs

1) Structural Modification of SWNTs: Fig. 4(a) shows a low-magnified FE-SEM image showing the typical morphology of the purified SWNTs. Most of the SWNTs are clean (not damaged) and uniformly distributed in the form of bundles with diameters ranging from approximately 5 to 50 nm. Although it has been reported that the ultrasonication or acidic washing treatment for SWNT's purification [14]–[16] and electron beam irradiation during TEM observation [17], [18] induce a considerable amount of structural defects on the nanotubes, any severe deformation is confirmed not to be found in our purified original samples, as shown in Fig. 4(b), which is obtained by FE TEM. The corresponding electron diffraction pattern is shown in the inset of Fig. 4(b). The relatively weak intensity along the circles is attributed to a random and continuous distribution of nanotube chiralities. However, it is found the armchair type nanotubes are somewhat dominant from the stressed equatorial line, which is perpendicular to bundle axis.

Raman scattering spectroscopy has been known as a convenient and powerful tool to investigate the nanotube diameter, structure, and electron properties. In Fig. 4(c), the typical contour of the Raman spectrum recorded using 488-nm wavelength is shown for the case of pure SWNTs. The spectrum consists of three main regimes as follows. Radial breathing band (R-band) in the low-frequency region of 150–250 cm $^{-1}$, disorder-induced band (D-band) observed around 1350 cm $^{-1}$, and graphite band (G-band) around 1590 cm^{-1}. Since Raman scattering takes place by a resonant coupling process between incident excitation frequency (wavelength) and electronic transition energies of the nanotubes, the R-band is strongly diameter dependent because the tube diameter is inversely proportional

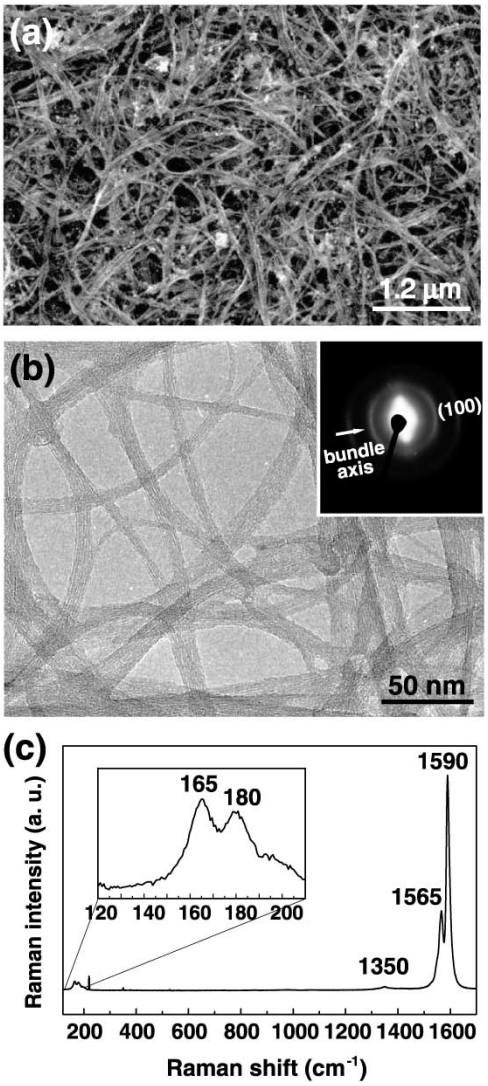

Fig. 4. Electron micrographs showing the purified SWNTs. (a) FE-SEM image. (b) FE-TEM image. Inset gives electron diffraction pattern of (b). (c) Typical Raman result recorded from the purified SWNTs. Inset in (c) gives magnified region of the low-frequency region.

to the electronic transition energy. Therefore, numerous calculations have been carried out to clarify the relation between the peaks in the R-band and tube diameters. Here, we adopt the generally known relation in order to estimate the distribution of the tube diameters $w = 223.75/d$ [w: wavenumber (cm^{-1}), d: individual tube diameter (nm)] [19]. According to this relation, the peaks at 165 and 180 cm^{-1}, which are presented in the inset of Fig. 4(c) are identified to correspond to the diameters of 1.36 and 1.24 nm, respectively. These values are somewhat smaller than those observed by the FE TEM, i.e., 1.0–2.0 nm. This deviation of the tube diameters between the Raman and TEM results is unavoidable due to their inherent difference of analyzing scope. Regarding the D-band, peaks are known to be associated with symmetry-lowering effects in disordered graphite. Namely, the peak intensity (I_D) is sensitive to the amount of disorder in carbon materials such as amorphous carbon, graphitic nanoclusters, or other defects. On the other hand, the G-band intensity (I_G) is related to graphite dispersion of the nanotube and characterized by peak splitting, which is different from the spectrum

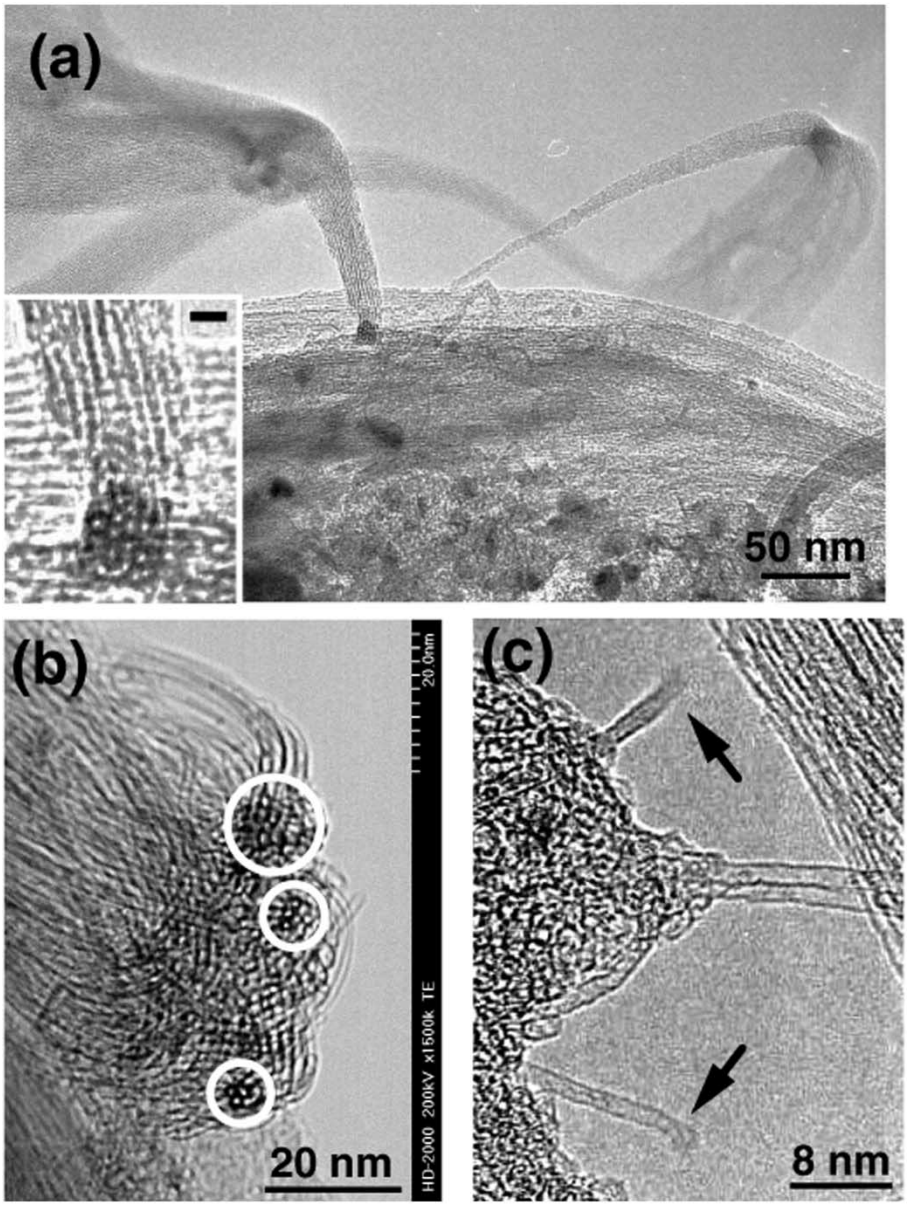

Fig. 5. (a) Representative FE-TEM image showing the structural deformed SWNTs irradiated by $\phi_{\rm ap} = -300$ V in Na $-$ C_{60} plasma. Inset of (a) shows a magnified image of the tube cut region and the scale bar is 4 nm. (b) STEM bright-field image shows deflected SWNT's bundles. Cross-sectional parts representing the triangular lattice are underlined by white circles. (c) FE-TEM image of open-ended tubes caused by plasma-ion irradiation. (b) and (c) Taken from the sample treated with the $\phi_{\rm ap} = -100$ V in Cs plasma.

of planar graphite [20]. For this reason, in order to estimate deformed nanotube structures quantitatively in relation to the applied bias-voltages ($\phi_{\rm ap}$), we introduce an intensity comparison of the Raman peaks (I_D/I_G) as a barometer. Throughout this paper, I_D/I_G refers to the ratio of the primary peak intensities of the D- and G-band, respectively.

When the positive bias ($\phi_{\rm ap} > 0$) is applied to the substrate covered with the dispersed SWNT bundles in the alkali-metal plasma, no appreciable structural change is observed in the TEM image. This means that the electron irradiation to the SWNT bundles is of no effect on its morphology. When the deeply negative bias ($\phi_{\rm ap} < 0$) is applied to the substrate, on the other hand, the extremely deformed SWNTs are clearly observed in the TEM image, as presented in Fig. 5. Fig. 5(a) taken from the specimen irradiated with the application of -300 V in the Na-fullerene plasma. We can find heavily deflected SWNT bundles with diameters of 10–50 nm and also the cross-sectioned image of SWNT bundle in an inset. When the deeply negative bias ($\phi_{\rm ap} < 0$) is applied to the substrate, the extremely deformed SWNTs are clearly observed in the TEM image, as presented in Fig. 5(b) and (c). Fig. 5(b) taken from the specimen irradiated with the application of -100 V in the Cs plasma shows deflected SWNT bundles and also presents the cross-sectioned image of bundles designated by white circles. Each small circle in those represents the cross section of an individual tube with a diameter $\sim$1.4 nm. A high-resolved FE-TEM image is also presented in Fig. 5(c), showing an open end due to cutting of the individual tube. These features are evidently different from the original morphology and well describe the situation as to how the SWNTs are changed after the plasma-ion irradiation. More-

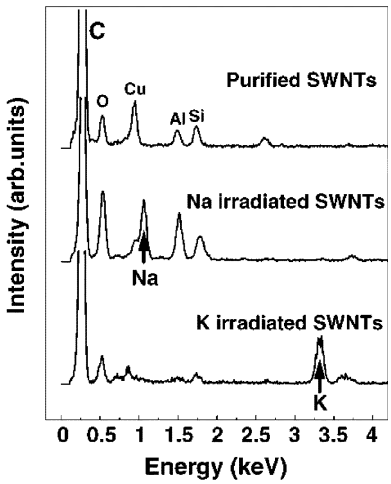

Fig. 6. Comparison of EDS spectra recorded from the purified (upper), Na irradiated (middle), and K irradiated (lower) SWNTs.

over, this change of the nanotube structure is enhanced with an increase in the ion acceleration energy ($-300\ \mathrm{V} < \phi_{\mathrm{ap}} < 0$).

According to EDS results, as shown in Fig. 6, alkali metals are confirmed to be well doped in the SWNT bundles in both the sodium (middle) and potassium (lower) plasmas, where a result of the sample before the plasma-ion irradiation (upper) is also compared. At this stage, however, it is impossible to determine whether the alkali elements are encapsulated inside the SWNTs or not. Therefore, Cs is selected as the dopant because of its large diameter (∼0.33 nm) and heavier weight, as compared to other alkali metals. The latter is advantageous to make the dopants easier to be detected by the STEM technique, while the former is beneficial for doping only through the open end (not via the tube wall) and for the stability of a junction configuration.

2) Cesium Encapsulation Inside SWNTs: Although many attempts have thus far been challenged to identify encapsulated materials inside the SWNTs, successful results reported are few. The Z-contrast technique by STEM is very useful for characterizing chemical elements spatial distribution at the atomic scale. Fan *et al.* have recently reported that iodine atoms intercalated by capillary wetting method inside SWNTs are encapsulated in the form of helical chains [21]. It is generally known that large contrast differences in the Z-contrast image originate from the intensity differences of high-angle scattered electrons [22], which are proportional to the square of atomic number (e.g., C = 6 and Cs = 55, in our case).

Fig. 7 clearly reveals the difference between the outside adsorption and inside encapsulation of Cs. Fig. 7(a) shows the thin bundle composed of 2–3 individual nanotubes, which illuminates very brightly due to the Cs presence in Fig. 7(b), bridging two thick bundles. The arrows in Fig. 7(c) and (d) designate the junction point between hollow (left-hand side) and Cs filled (right-hand side) regions of the SWNT. These figures imply a very important fact that Cs ions did not enter the nanotube presumably through the sidewall. From the geometric point-of-view, it is very much easier to enter through the open end (diameter of 1–2 nm) rather than sidewall (diameter of 0.25 nm) of the tube. Moreover, if the Cs positive ion (diameter of 0.33 nm) is encapsulated through the sidewall, it is impossible to explain why this clear junction point can be made. Namely, if Cs is attached around the tube wall and enters the inner space, it is very hard to consider why Cs does not distribute uniformly over the entire tube, such as shown in Fig. 7(a) and (b). From these reasons, we finally conclude that the Cs intercalation takes place via open ends.

Fig. 8 gives high-resolved FE-TEM images, corresponding schematic illustrations, and EDS results obtained from the sample treated with $\phi_{\mathrm{ap}} = -100$ V. The linear and spiral configurations of intercalated Cs are clearly shown in Fig. 8(a) and (b), respectively. An inset in Fig. 8(a) stresses the intercalated Cs denoted by dotting with black circles and the bottom image in Fig. 8(b) is also marked by dotting for a spiral chain of intercalated Cs inside the individual nanotube bridging two nanotube bundles. In Fig. 8(c), on the other hand, we can find two or three individual nanotubes combined with each other via Van der Waals attraction. Although the upper tube looks vacant, the lower tube is observed to be partially intercalated. An inset especially reveals the regularly located two rows of Cs.

Here, when we suppose the case of Cs^+ intercalation inside the $(10, 10)$ nanotube, which is the most general tube, the Cs array as in Fig. 8(c) is basically possible according to their simple geometry. The diameter of the $(10, 10)$ tube is generally known to be approximately 13.6 Å, and the π electron-cloud thickness is considered to be 1.7 Å. Therefore, the inner space of the $(10, 10)$ tube is approximately 10.2 Å as a diameter. Judging from this structural comparison, there still remains room of 3.52 Å between two rows of Cs^+ having the 3.34-Å diameter. Strictly speaking, the accurate encapsulation site of Cs^+ has to be determined on the basis of the comprehensive understanding of the detail of interaction energy between the tube wall and intercalant, which is governed by the competition between Van der Waals and coulomb forces.

Concerning this point about Cs encapsulation, some results have recently been published elsewhere [23]. In any case, the result well indicates the existence of Cs in the irradiated SWNTs, as shown in Fig. 8(d). Here, in order to obtain an accurate compositional information from a localized and isolated SWNT bundle composed of 4–5 individual tubes, the electron beam size is compressed (∼5-nm diameter) in the EDS analysis, which inevitably yields a relatively weak intensity of the Cs spectrum peak.

B. Alkali–Fullerene Plasma-Ion Irradiation to SWNTs

1) Formation of Fullerene Encapsulated SWNTs: On the other hand, when the alkali–fullerene plasma instead of the alkali-metal plasma is used, more drastic changes of the SWNTs are observed, as demonstrated in the TEM images of Fig. 9(a) and (b), which are obtained from the samples treated in the range of the positive-bias application ($\phi_{\mathrm{ap}} = 5$–20 V) in the alkali–fullerene plasma. From these images, we can clearly find the isolated SWNTs containing a self-assembled or set of fullerene molecules, as well as modified morphology. Fig. 9(a) and (b) presents direct evidence that the fullerenes are well intercalated, presumably through the tube kink region [as shown in the inset of Fig. 9(a)] or open end [as shown in Fig. 9(b)] of the SWNTs. Actually, these features can easily be

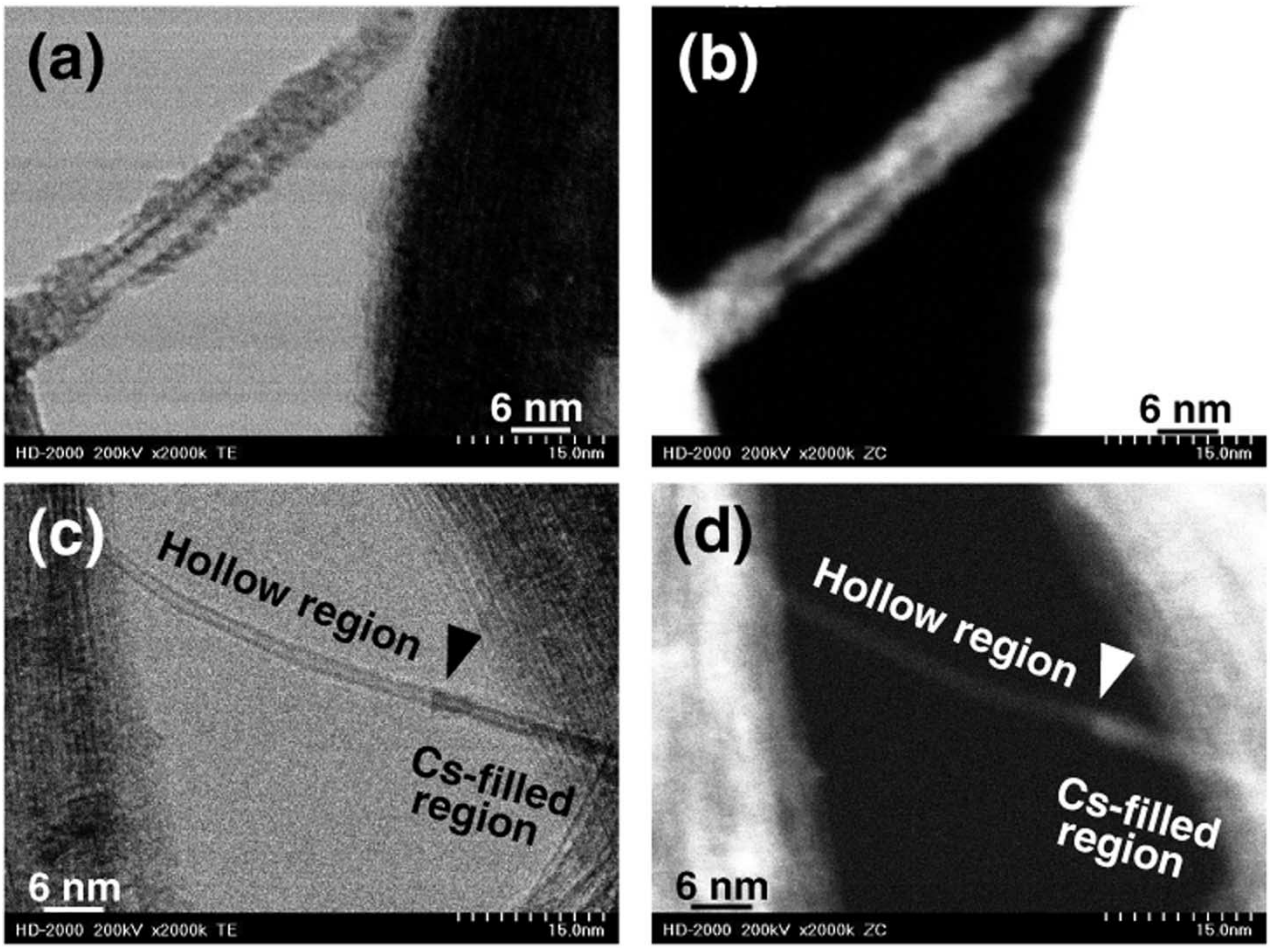

Fig. 7. (a) Bright-field STEM image of Cs adsorbed SWNTs. (b) Z-contrast image corresponding to (a). (c) Bright-field STEM image of Cs filling inside individual nanotube. (d) Z-contrast image corresponding to (c).

found from many samples treated with the similar conditions of the bias application in the alkali–fullerene plasma. This is evidently due to the accelerated C_{60}^- impact toward the SWNT bundles because such a TEM image is never observed for the positive-bias application in the alkali-metal plasma. More interestingly, we have no structural deformation in the range of $\phi_{\rm ap} = 5$–20 V in cases of DWNTs, TWNTs, and MWNTs. However, we have obtained quite different results after C_{60}^- irradiation in the case of $\phi_{\rm ap} = 50$ V or $\phi_{\rm ap} = 100$ V. Fig. 9(c) and (d) presents the representative high-resolved FE-TEM images of the DWNT and MWNT irradiated by $\phi_{\rm ap} = 50$ V and 100 V, respectively. We can clearly see the features of mechanically broken, and therefore, open-ended DWNTs/MWNTs. It is possible to conjecture from the images that the destructions of the nanotube structures are caused by mechanical impact such as accelerated C_{60}^- bombardment that we suggested in the case of SWNTs just before. In case of MWNTs, which are grown by plasma-enhanced chemical vapor deposition and are expected to exhibit higher mechanical strength than that of DWNTs due to their numerous layers, the structural deformation is observed for $\phi_{\rm ap} = 100$ V (not shown here).

Fig. 10, obtained from the samples of $\phi_{\rm ap} = 20$ V in the $Cs^+ - C_{60}^-$ plasma, shows various FE-TEM images of fullerene encapsulated SWNTs and TWNTs, i.e., so-called C_{60} peapods. The C_{60} molecules having a diameter of 0.71 nm are separated from the SWNT walls by a van der Waals distance of $\sim$0.35 nm. Therefore, the geometry of spherical C_{60} molecules would be the most suitable structure for encapsulation into general SWNTs. Completely filled nanotubes by close-packed fullerenes are presented in Fig. 10(a). Since the focal plane in the FE TEM is different along the nanotube, it is natural that the fullerene molecules look like they are being attached to each other. The protruding nanotube tip has an unusual morphology, not hemisphere, which means the nanotube has undergone some structural deformation. A more interesting feature is shown in Fig. 10(b). This SWNT bundle is also composed of two individual tubes, such as that shown in Fig. 10(a). In Fig. 10(b), although the lower tube seems to contain something in the inner space, it is actually not the intercalants, but the impurities such as carbon fragments, carbonaceous matters, etc. These impurities generally decorate the nanotube surrounding and are observed frequently in the TEM images. On the other hand, we can clearly confirm the upper tube incorporates a fullerene chain through its open end (black arrow). Fig. 10(c), which presents frequently observed features in this study, provides strong evidence that the fullerenes are well intercalated in the case of using our plasma irradiation method. Concerning TWNTs, we have also confirmed spherical materials indicated by a black arrow in Fig. 10(d), which are encapsulated into the inner space of TWNTs in the case of $\phi_{\rm ap} = 100$ V.

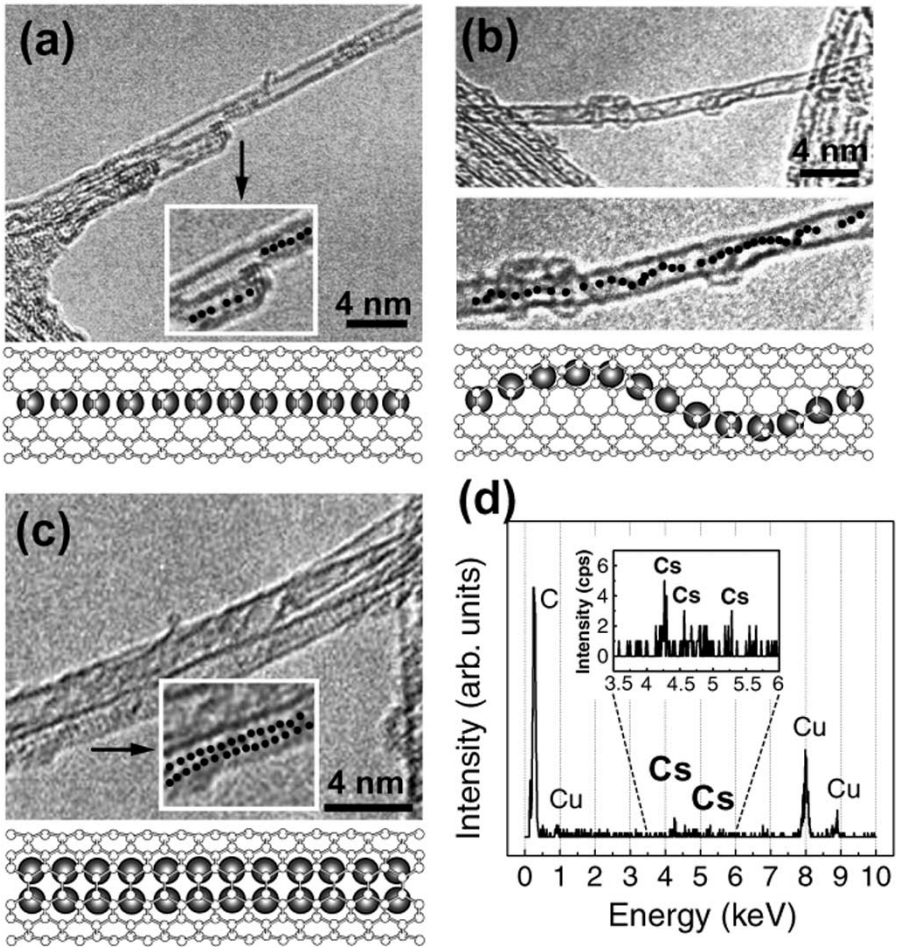

Fig. 8. (a)–(c) High-resolved FE-TEM images and their corresponding illustrations. (d) EDS spectrum obtained from the samples treated with the $\phi_{\rm ap} = -100$ V in the Cs plasma. (a) Linear configuration of intercalated Cs. The inset underlines the intercalated Cs by dotting with black circles. (b) Helical shape of encapsulated Cs inside the individual nanotube bridging two bundles. The upper image is original and the bottom is a marked image by dotting the Cs trace. (c) The lower tube is partially intercalated and presumably crystallized. The inset emphasizes the crystallization of Cs. (d) EDS result recorded from very thin bundles, each of which is composed of 4–5 individual tubes, and reveals the Cs existence.

Fig. 11(a) shows a quantitative relationship between the plasma density used and the production rate of C_{60} peapods. In the case of $Li^+ - C_{60}^-$ plasma (5×10^8 cm^{-3} $< n_e <$ 5×10^9 cm^{-3}), the fullerene encapsulation rate is placed between 20%–25%. On the other hand, the encapsulation yield is raised up to 60%–70% in the case of $Cs^+ - C_{60}^-$ plasma ($n_e > 10^{10}$ cm^{-3}). This C_{60} encapsulation yield is estimated on the basis of the length of encapsulated parts to the total length of clearly discernible nanotubes from so many high-resolved images taken by FE TEM. It is found that the encapsulation rate linearly increases with an enhancement of the plasma density. This is reasonable that higher plasma density means more increased irradiation ion flux, which may be crucial in the enhancement of the encapsulation rate.

2) Proposed Model of "Structural Modification and Consecutive Material Encapsulation Into the SWNTs" due to Plasma-Ion Irradiation: Since the strong electric field $E_{||}$ parallel to the magnetic-field lines is formed in the plasma-sheath region just in front of the biased substrate, SWNT bundles would be oriented elastically in the direction of the electric field due to the concentration of induced charges at the tip of the SWNT bundles. Here, the thickness of the plasma sheath (d) depends on the plasma density (n_e), temperature (T_e), and absolute value of the substrate bias ($|\phi_{\rm ap}|$). For instance, $d \approx 3.84$ mm for $n_e = 10^9$ cm^{-3}, $T_e \approx 0.2$ eV, and $|\phi_{\rm ap}| = 100$ V ($E_{||||} \approx 2.7 \times 10^2$ V/cm). Recently, Poncharal *et al.* has demonstrated the physical and mechanical properties of individual nanotubes using such an electrostatic deflection phenomenon [24]. Furthermore, in our plasma system, numerous charged ions with accelerated velocities simultaneously bombard the aligned SWNT bundles from the side direction because of their large Larmor radii compared with the bundle diameters (~100 nm), possibly resulting in the irreversible deformation described in Fig. 5. According to the above-mentioned scenario, the positive-bias application in the alkali–fullerene plasma is conjectured to enhance the structure deformation of the SWNTs more because the momentum transfer from ions to SWNT bundles is proportional to the root of ion mass for a fixed $\phi_{\rm ap}$. The absolute value of $\phi_{\rm ap}$ for the SWNT's deformation or fullerene filling in the case of the alkali–fullerene plasma is much smaller ($|\phi_{\rm ap}| < 20$ V, as shown in Fig. 9) than that in the alkali-metal plasma ($|\phi_{\rm ap}| > 100$ V, as shown in Fig. 5). The irradiation ion velocity is given by $v = (2e|\phi|/m)^{1/2}$ because the kinetic energy is described by

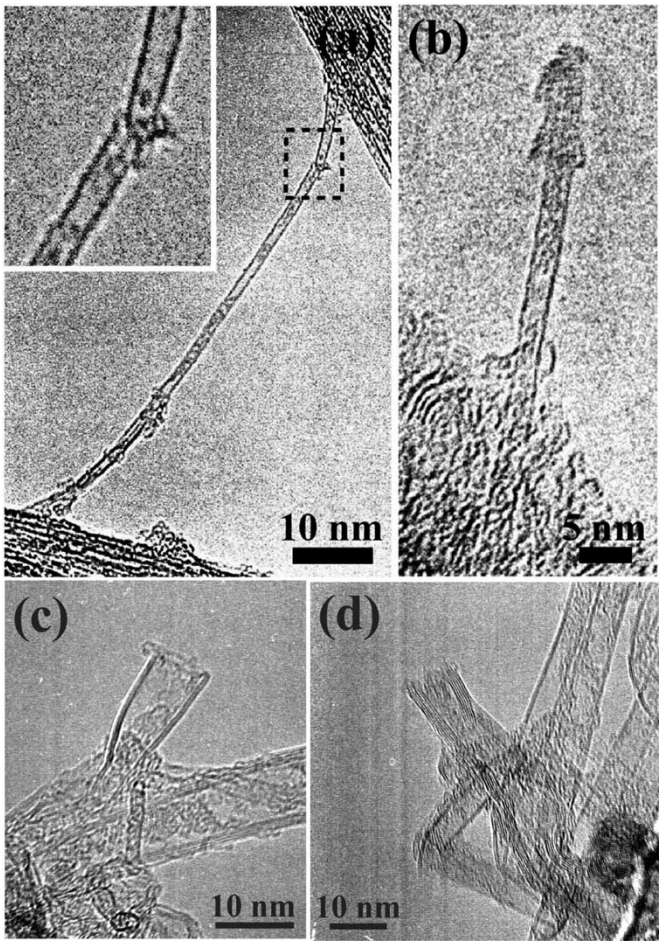

Fig. 9. FE-TEM images showing that the C_{60} encapsulated SWNTs are obtained from the samples treated with the: (a) $\phi_{\rm ap} = 10$ V in $Li - C_{60}$ plasma and (b) $\phi_{\rm ap} = 20$ V in $Na - C_{60}$ plasma. (c) and (d) Representative high-resolved FE-TEM images of C_{60} irradiated DWNTs. (c) $\phi_{\rm ap} = 50$ V and (d) $\phi_{\rm ap} = 100$ V.

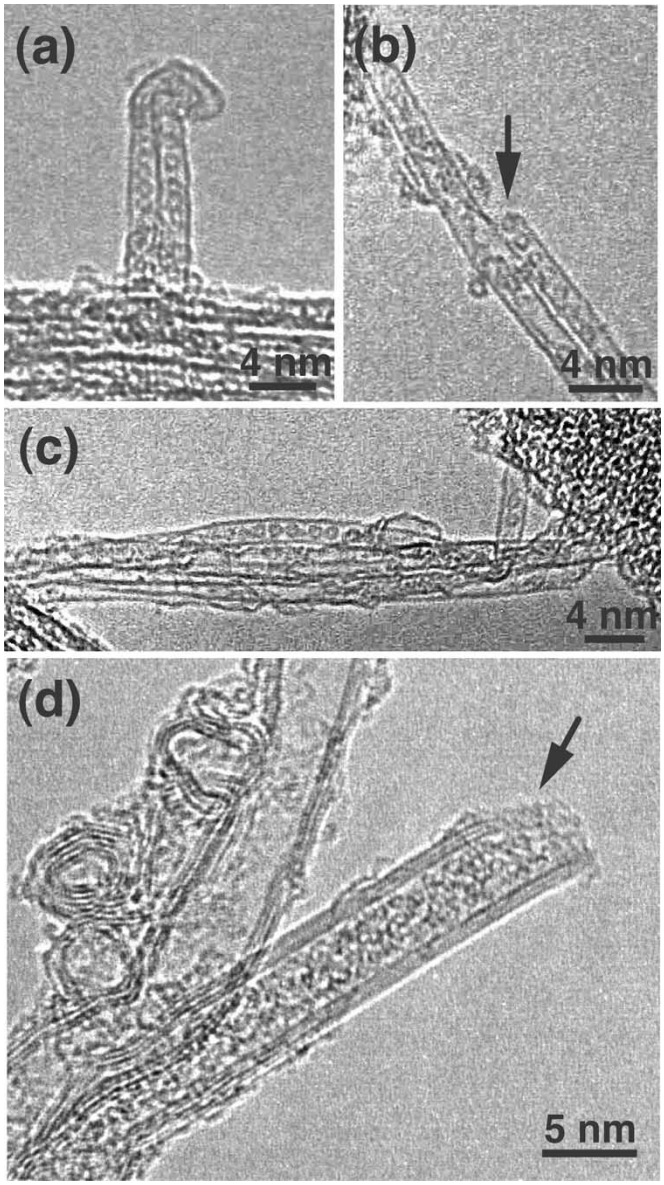

Fig. 10. High-resolved FE-TEM images demonstrating: (a) completely filled nanotubes by close-packed fullerenes and showing (b) the fullerenes are incorporated through its open end (black arrow). (c) Typical features of fullerene peapods formed by plasma-ion irradiation method. (d) The open-ended DWNT is filled with spherical materials, which are indicated by a black arrow and expected to be C_{60}.

$mv^2/2 = e|\phi|$, where ϕ is the difference between the plasma potential ϕ_p and $\phi_{\rm ap}(\phi = \phi_p - \phi_{\rm ap})$. Since $|\phi_{\rm ap}|$ is much larger than $|\phi_p|$, it is reasonable that the root of mass ratio between positive and negative ions is directly proportional to the root of the applied-bias ratio $(m_+/m_-)^{1/2} \approx (-\phi_{\rm ap(-)}/\phi_{\rm ap(+)})^{1/2}$. Here, m_+ denotes the mass of positive alkali-metal ions (7, 23, 39, and 133 for Li^+, Na^+, K^+, and C^+, respectively), m_- denotes the mass of negative fullerene ions (720 for C_{60}^-), $\phi_{\rm ap(+)}$ denotes the applied bias in the case of positive alkali-metal ion irradiation, and $\phi_{\rm ap(-)}$ denotes the applied bias in the case of negative C_{60} ion irradiation. Namely, the degree of the structural modifications in our experimental system is closely related to the mass of accelerated charged particles to the nanotubes.

Our structural deformation and consecutive encapsulation mechanism mentioned just above is also again strongly supported by a good agreement of the TEM results with the Raman results, as given in Fig. 11(b). It is found that the value of I_D/I_G increases with increasing the absolute value of an applied bias-voltage, which is a key parameter to determine the plasma-ion irradiation energy. In other words, the amount of disordered nanostructures induced by tube bending or tube cutting increases due to the increased ion irradiation energy because the D-band in the Raman spectra is activated from the scattering process by the presence of in-plane defects. Moreover, the value of I_D/I_G at the same substrate bias voltage is relatively well ordered with their atomic masses. A more interesting fact is the value of I_D/I_G of C_{60} irradiation by $\phi_{\rm ap} = 10$ or 20 V application in the $Li^+ - C_{60}^-$ plasma (gray region), which is much higher than that of the case of positive alkali-metal irradiation.

Therefore, considering all these results, we can confidently conclude that these modified nanotube structures in our experimental system are mainly produced by momentum transfer from the accelerated charged particles to the nanotubes and may contribute to yielding an enhanced encapsulation of intercalants inside the SWNTs.

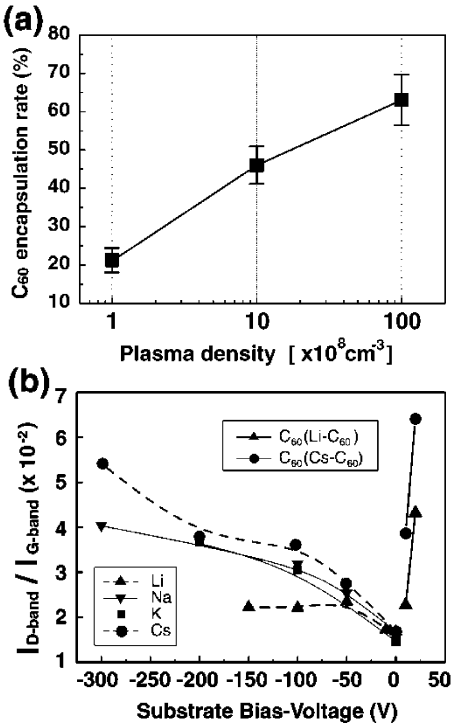

Fig. 11. (a) Quantitative relationship between alkali–fullerene plasma density and C_{60} encapsulation yield. The encapsulation rate linearly increases with an enhancement of the plasma density. (b) Variations of I_D/I_G values for substrate bias voltage.

IV. Conclusion

The bias-voltage application to SWNTs in plasmas mainly consisting of positive and negative ions has been evidenced to be an effective method for the synthesis of SWNTs encapsulating various types of foreign atoms. In a series of experiments on this new approach, in contrast to purified samples, a remarkable change of the nanotube structure is observed after the plasma-ion irradiation at the first stage. The Cs encapsulation are then realized for the first time by the negative-bias application leading to ion irradiation to SWNTs. In the case of the positive bias application in the alkali–fullerene plasma, C_{60} encapsulated SWNTs are found to be effectively synthesized. When we make a comparison of absolute values of the applied bias, yielding appreciable structural modifications, it is clarified that the structural modification after the ion irradiation is mainly caused by ion-momentum transfer to the nanotubes. Finally, an extension of this study is expected to lead to the development of a unique nanotechnology through the creation of novel functional nanomaterials.

Acknowledgment

The authors would like to thank K. Tohji, Y. Kawazoe, K. Motomiya, and T. Yaguchi for their support.

References

[1] H. W. Kroto, J. R. Heath, S. C. O'Brien, R. F. Curl, and R. E. Smalley, "C_{60}: Buckminsterfullerene," *Nature*, vol. 318, pp. 162–163, 1985.
[2] S. Iijima, "Helical microtubules of graphitic carbon," *Nature*, vol. 354, pp. 56–58, 1991.
[3] S. Iijima and T. Ichihashi, "Single-shell carbon nanotubes of 1-nm diameter," *Nature*, vol. 363, pp. 603–605, 1993.
[4] R. S. Lee, H. J. Kim, J. E. Fischer, A. Thess, and R. E. Smalley, "Conductivity enhancement in single-walled carbon nanotube bundles doped with K and Br," *Nature*, vol. 388, pp. 255–257, 1997.
[5] J. Kong, N. R. Franklin, C. Zhou, M. G. Chapline, S. Peng, K. Cho, and H. Dai, "Nanotube molecular wires as chemical sensors," *Science*, vol. 287, pp. 622–625, 2000.
[6] J. Lee, H. Kim, S. J. Kahng, G. Kim, Y. W. Son, J. Ihm, H. Kato, Z. W. Wang, T. Okazaki, H. Shinohara, and Y. Kuk, "Bandgap modulation of carbon nanotubes by encapsulated metallofullerenes," *Nature*, vol. 415, pp. 1005–1008, 2002.
[7] K. Esfarjani, A. A. Farajian, Y. Hashi, and Y. Kawazoe, "Electronic and transport properties of N–P doped nanotubes," *Appl. Phys. Lett.*, vol. 74, pp. 79–81, 1999.
[8] N. Sato, T. Mieno, T. Hirata, Y. Yagi, R. Hatakeyama, and S. Iizuka, "Production of C_{60} plasma," *Phys. Plasmas*, vol. 1, pp. 3480–3484, 1994.
[9] R. W. Motley and T. Kawabe, "Energy analysis of cesium ions in a Q machine," *Phys. Plasmas*, vol. 14, pp. 1019–1023, 1971.
[10] F. F. Chen, *Introduction to Plasma Physics and Controlled Fusion*, 2nd ed. New York: Plenum, 1984, pp. 290–296.
[11] J. L. Hutchison, N. A. Kiselev, E. P. Krinichnaya, A. V. Krestinin, R. O. Loutfy, A. P. Morawsky, V. E. Muradyan, E. D. Obraztsova, J. Sloan, S. V. Terekhov, and D. N. Zakharov, "Double-walled carbon nanotubes fabricated by a hydrogen arc discharge method," *Carbon*, vol. 39, pp. 761–770, 2001.
[12] T. Hirata, N. Satake, G.-H. Jeong, T. Kato, R. Hatakeyama, K. Motomiya, and K. Tohji, "Magnetron-type radio-frequency plasma control yielding vertically well-aligned carbon nanotube growth," *Appl. Phys. Lett.*, vol. 83, pp. 1119–1121, 2003.
[13] K. Tohji, T. Goto, H. Takahashi, Y. Shinoda, N. Shimizu, B. Jeyadevan, I. Matsuoka, Y. Saito, A. Kasuya, T. Ohsuna, K. Hiraga, and Y. Nishina, "Purifying single-walled nanotubes," *Nature*, vol. 383, p. 679, 1996.
[14] K. L. Lu, R. M. Lago, Y. K. Chen, M. L. H. Green, P. J. F. Harris, and S. C. Tsang, "Mechanical damage of carbon nanotubes by ultrasound," *Carbon*, vol. 34, pp. 814–816, 1996.
[15] K. B. Shelimov, R. O. Esenaliev, A. G. Rinzler, C. B. Huffman, and R. E. Smalley, "Purification of single-wall carbon nanotubes by ultrasonically assisted filtration," *Chem. Phys. Lett.*, vol. 282, pp. 429–434, 1998.
[16] Z. Jia, Z. Wang, J. Liang, B. Wei, and D. Wu, "Production of short multi-walled carbon nanotubes," *Carbon*, vol. 37, pp. 903–906, 1999.
[17] P. M. Ajayan, V. Ravikumar, and J. C. Charlier, "Surface reconstructions and dimensional changes in single-walled carbon nanotubes," *Phys. Rev. Lett.*, vol. 81, no. 7, pp. 1437–1440, 1998.
[18] C. Kiang, "Electron irradiation induced dimensional change in bismuth filled carbon nanotubes," *Carbon*, vol. 38, pp. 1699–1701, 2000.
[19] S. Bandow, S. Asaka, Y. Saito, A. M. Rao, L. Grigorian, E. Richter, and P. C. Eklund, "Effect of the growth temperature on the diameter distribution and chirality of single-wall carbon nanotubes," *Phys. Rev. Lett.*, vol. 80, pp. 3779–3782, 1998.
[20] R. Saito, G. Dresselhaus, and M. S. Dresselhaus, *Physical Properties of Carbon Nanotubes*. London, U.K.: Imperial College Press, 1998, pp. 187–192.
[21] X. Fan, E. C. Dickey, P. C. Eklund, K. A. Williams, L. Grigorian, R. Buczko, S. T. Pantelides, and S. J. Pennycook, "Atomic arrangement of iodine atoms inside single-walled carbon nanotubes," *Phys. Rev. Lett.*, vol. 84, no. 20, pp. 4621–4624, 2000.
[22] P. D. Nellist and S. J. Pennycook, "Direct imaging of the atomic configuration of ultradispersed catalysts," *Science*, vol. 274, pp. 413–415, 1996.
[23] G.-H. Jeong, A. A. Farajian, R. Hatakeyama, T. Hirata, T. Yaguchi, K. Tohji, H. Mizuseki, and Y. Kawazoe, "Cesium encapsulation in single-walled carbon nanotubes via plasma ion irradiation: Application to junction formation and *ab initio* investigation," *Phys. Rev. B, Condens. Matter*, vol. 68, pp. 075 410-1–075 410-6, 2003.
[24] P. Poncharal, Z. L. Wang, D. Ugarte, and W. A. Heer, "Electrostatic deflections and electrochemical resonances of carbon nanotubes," *Science*, vol. 283, pp. 1513–1516, 1999.

Rikizo Hatakeyama was born in Akita, Japan, on April 25, 1947. He received the B.E., M.E., and Ph.D. degrees in electronic engineering from Tohoku University, Sendai, Japan, in 1971, 1973, and 1976, respectively.

He is currently a Professor with the Department of Electronic Engineering, Tohoku University. His research interests encompass experiments not merely on fundamental plasma physics, but also nanocarbon material developments using plasma technology.

Goo-Hwan Jeong was born in Chung-book, Korea, on August 1, 1971. He received the B.E. and M.E. degrees in metallurgical engineering from In-Ha University, Inchon, Korea, in 1997 and 1999, respectively, and the Ph.D. degree in electronic engineering from Tohoku University, Sendai, Japan, in 2003.

He is currently a Research Fellow with the Japan Society for the Promotion of Science (JSPS), Department of Electronic Engineering, Tohoku University. His research interest is nanomaterial development using plasma technology and their application.

Takamichi Hirata was born in Hukushima, Japan, on August 20, 1965. He received the B.E. and M.E. degrees in electric engineering from Iwate University, Iwate, Japan, in 1990 and 1992, respectively, and the Ph.D. degree in electric engineering from Tohoku University, Sendai, Japan, in 2001.

He is currently a Lecturer with the Department of Electronic Engineering, Tohoku University. His research interests are fundamental experiments on fullerene plasmas and fullerene-based nanomaterial synthesis using plasma technology.